ADVANCED ELECTRONIC MATERIALS
www.advelectronicmat.de

Check for updates

A Current–Voltage Model for Double Schottky Barrier Devices

*Alessandro Grillo and Antonio Di Bartolomeo**

Schottky barriers (SBs) are often formed at the semiconductor/metal contacts and affect the electrical behavior of semiconductor devices. In particular, SBs are playing a major role in the investigation of the electrical properties of mono and 2D nanostructured materials, although their impact on the current–voltage characteristics is frequently neglected or misunderstood. In this work, a single equation is proposed to describe the current–voltage characteristics of two-terminal semiconductor devices with Schottky contacts. The equation is applied to numerically simulate the electrical behavior for both ideal and nonideal SBs. The proposed model can be used to directly estimate the SB height and the ideality factor. It is applied to perfectly reproduce the experimental current–voltage characteristics of ultrathin molybdenum disulfide or tungsten diselenide nanosheets and tungsten disulfide nanotubes. The model constitutes a useful tool for the analysis and the extraction of relevant transport parameters in any two-terminal device with Schottky contacts.

1. Introduction

Current–voltage (I–V) measurements are an efficient way for evaluating the quality of metal contacts and for the extraction of fundamental parameters such as the Schottky barrier (SB) height and the contact resistance. To study the I–V characteristic of two terminal devices with SBs, the classic equation of the Schottky diode is often used. This equation considers that charge carriers cross an energy barrier by thermionic emission. In this approach, it is implicitly assumed that there is a Schottky junction at the forced contact while the other contact is Ohmic. Moreover, in such an approach, only the dominant current, occurring either at positive or negative voltages, is commonly used to evaluate the barrier parameters. Nevertheless, in most devices both contacts have a rectifying nature and the simplistic assumption of a single SB leads to the wrong results, such as very large ideality factors ($n \gg 1$) or unrealistic SB height and Richardson constant.

Oldham and Milnes highlighted the need to consider two barriers to describe the electric conduction based on thermionic emission in n–n heterojunctions.[1] Then, Ramirez et al.[2] and Nagano et al.[3] applied the model to study the electric transport in SnO_2 nanowires and in C_{60} films with Au contacts. In both works, the authors did not consider that barriers with different heights could form at the contacts. Such a possibility might easily occur as the SB height is related to interfacial chemistry and local defects. Nouchi proposed a single equation[4] to study the SB of a device formed by a metal–semiconductor junction, in which a second electrode necessary to perform the electrical measurement forms a metal–semiconductor–metal structure. This model does not consider the possibility that the two SBs formed with the contacts may have different ideality factors and requires the use of the first and second derivative of the I–V characteristic of the device that can limit its applicability. A model with two different barriers at the contacts was proposed by Chiquito et al. who limited their study to the analysis of metal/SnO_2/metal devices.[5] A model based on SBs with different heights was used by Di Bartolomeo et al. to account for the rectifying electrical characteristics observed in field effect transistors with ultrathin transition-metal dichalcogenide channel[6,7] or in metal/insulator/semiconductor structures.[8]

In this work, we apply a simple model to describe the conduction in a two-terminal device in which two rectifying contacts are present. The model allows extracting both SB heights simultaneously. First, we use the model to make numerical simulations of the I–V curves for different combination of junction parameters such as barrier height, area, and ideality factor.[9] Then, we test the model fitting the symmetric or asymmetric I–V curves of two-terminal nanodevices made of molybdenum disulphide (MoS_2) or tungsten diselenide (WSe_2) nanosheets and tungsten disulphide (WS_2) nanotubes. MoS_2, WSe_2, and WS_2 are major exponents of the transition metal dichalcogenides, a family of layered materials with promising technological applications.[6,7,10–12] We highlight that, although demonstrated for nanostructured semiconductors, the model can be applied to any devices with two SBs.

A. Grillo, Prof. A. Di Bartolomeo
Physics Department "E. R. Caianiello" and Interdepartmental Center "Nanomates"
University of Salerno
via Giovanni Paolo II n. 132, Fisciano 84084, Italy
E-mail: adibartolomeo@unisa.it

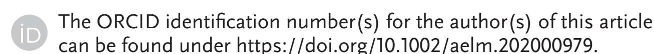
The ORCID identification number(s) for the author(s) of this article can be found under https://doi.org/10.1002/aelm.202000979.

DOI: 10.1002/aelm.202000979

 © 2020 Wiley-VCH GmbH

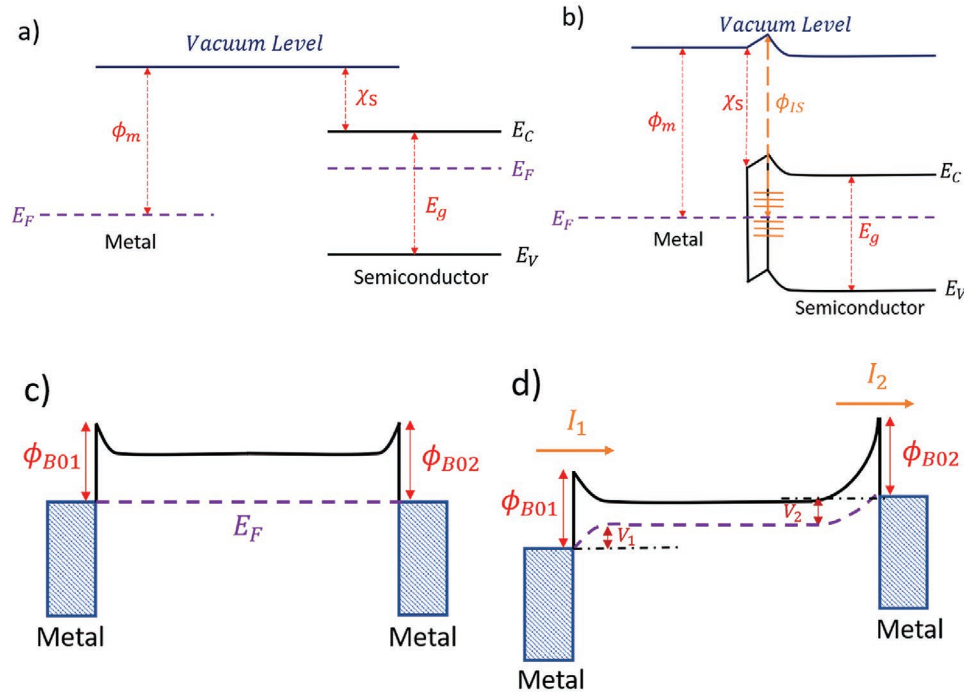

Figure 1. a) Typical band diagram of a metal and an n-type semiconductor before they are brought into contact. b) Band diagram of a metal in contact with a semiconductor where a high density of interface states is present. The Fermi level is pinned at the semiconductor interface state, ϕ_{IS}, and the SB height is independent of the metal work function. c) Energy diagram of a semiconductor with two Schottky junctions at the contacts for unbiased condition. d) Energy diagram of the same device when an external potential V is applied to the left contact. I_1 and I_2 represent the current through the two barriers, while V_1 and V_2 are the potential drops at the junctions ($V = V_1 + V_2$). The dashed violet line represents the quasi-Fermi level.

2. Experimental Section

The SB height is defined as

$$\begin{aligned} \phi_{SB-n} &= \phi_m - \chi_s \\ \phi_{SB-p} &= E_g + \chi_s - \phi_m \end{aligned} \tag{1}$$

where ϕ_{SB-n} and ϕ_{SB-p} are the SB heights for electron and hole injection, respectively, ϕ_m is the metal work function, χ_s is the semiconductor electron affinity, and E_g is the bandgap of the semiconductor, as shown in **Figure 1**a. According to Equation (1), a low work function metal with the Fermi level close or above the bottom of the conduction band of the semiconducting material facilitates the electron injection whereas a high work function metal with the Fermi level close or below the valence band of the material favors the hole injection. However, Equation (1) gives only qualitative indications of the SB heights and is rarely in quantitative agreement with the experimental data. This is mainly because the metal Fermi level can be pinned at a semiconductor interface state, ϕ_{IS}, if a high density of interface states is formed within the semiconductor bandgap during the fabrication process, as shown in Figure 1b. In this case, the equation for ϕ_{SB-n} is replaced by[13]

$$\phi_{SB-n} = (S \cdot \phi_m - \chi_s) + (1 - S)\phi_{IS} \tag{2}$$

where $S = \dfrac{\partial \phi_{SB-n}}{\partial \phi_M}$ is the Schottky pinning factor (a similar expression is used for ϕ_{SB-p}). If $S = 0$, the pinning is maximum, the SB turns out to be independent of the metal work function, and the so-called Bardeen limit is reached. Conversely, when $S = 1$, the Bardeen limit converges to the Schottky limit, represented by Equation (1).

Since the evaluation of the Schottky pinning factor and the semiconductor interface state energy, ϕ_{IS}, is complicated by variability of the fabrication process, the extraction of the SB height by means of electrical measurements is one of the most efficient techniques of investigation.

Usually, when a semiconductor material is measured in standard two-probe configuration, the grounded contact is assumed Ohmic while the other contact can form a Schottky junction regulated by a potential barrier. This assumption is unrealistic because Schottky junctions can be formed at both contacts. Hence, to approach the problem in a more general way, we assume that there are SBs at both metal contacts with the semiconductor.

If no external potential is applied, the band diagram of the device with two Schottky contacts is shown in Figure 1c in which the two barriers are designated as ϕ_{B01} and ϕ_{B02}, respectively. When a positive potential V (bias) is applied to the left contact, the bands are bent as shown in Figure 1d. We indicate with $V_{1,2}$ and $I_{1,2}$ the potential drop and the currents at the contacts 1 and 2, respectively.

We note that the semiconductor with SBs at both contacts can be modeled with two back-to-back Schottky diodes separated by a series resistance. When a sufficiently high external voltage is applied, whether positive or negative, one Schottky junction is forward-biased while the other one is reverse-biased.

 © 2020 Wiley-VCH GmbH

2199160x, 2021, 2, Downloaded from https://onlinelibrary.wiley.com/doi/10.1002/aelm.202000979 by Universita Di Salerno, Wiley Online Library on [20/01/2025]. See the Terms and Conditions (https://onlinelibrary.wiley.com/terms-and-conditions) on Wiley Online Library for rules of use; OA articles are governed by the applicable Creative Commons License

The reverse saturation current of the reverse-biased diode always limits the current.

Based on thermionic emission, the current at the two contacts can be written as[9]

$$I_1 = I_{s1}\left[e^{\frac{qV_1}{kT}} - 1\right] \tag{3}$$

$$I_2 = -I_{s2}\left[e^{-\frac{qV_2}{kT}} - 1\right] \tag{4}$$

where

$$I_{s1,s2} = S_{1,2}\, A^* T^2 \exp\left(-\frac{\phi_{B01,2}}{kT}\right) \tag{5}$$

are the reverse saturation currents, A^* is the Richardson constant, T is the temperature, k is the Boltzmann constant, and $S_{1,2}$ are the areas of the junctions. For the continuity of the current, the total current I_T can be expressed as $I_T = I_1 = I_2$, while the applied potential is $V = V_1 + V_2$. Starting from $I_T = I_1$, we have

$$I_T = I_{s1}\left[e^{\frac{qV_1}{kT}} - 1\right] \tag{6}$$

and substituting $V_1 = V - V_2$

$$I_T = I_{s1}\left[e^{\frac{qV}{kT}} e^{-\frac{qV_2}{kT}} - 1\right] \tag{7}$$

Using Equation (4), the term $e^{-\frac{qV_2}{kT}}$ can be expressed as

$$e^{-\frac{qV_2}{kT}} = 1 - \frac{I_2}{I_{s2}} = 1 - \frac{I_T}{I_{s2}} \tag{8}$$

since $I_2 = I_T$. Then, substituting Equation (8) into Equation (7), it results

$$I_T = I_{s1}\left[e^{\frac{qV}{kT}}\left(1 - \frac{I_T}{I_{s2}}\right) - 1\right] \tag{9}$$

Executing all the products and isolating I_T, we get

$$I_T = \frac{I_{s1}\left(e^{\frac{qV}{kT}} - 1\right)}{1 + \frac{I_{s1}}{I_{s2}} e^{\frac{qV}{kT}}} \tag{10}$$

Finally, multiplying numerator and denominator by $2I_{s2}e^{-\frac{qV}{2kT}}$, we obtain

$$I_T = \frac{2I_{s1}I_{s2}\sin h\left(\frac{qV}{2kT}\right)}{\left(I_{s1}e^{\frac{qV}{2kT}} + I_{s2}e^{-\frac{qV}{2kT}}\right)} \tag{11}$$

As it should be expected, Equation (11) is transformed into the single SB equation for a configuration with an SB and an Ohmic contact, for instance, when $\phi_{B01} \neq \phi_{B02} = 0$. This can be immediately understood considering, e.g., that when $\phi_{B02} = 0$ and $S_1 \approx S_2$, it results that

$$I_{s1}e^{\frac{qV}{2kT}} = S_1\, A^* T^2 e^{-\frac{\phi_{B01,2}}{kT}} e^{\frac{qV}{2kT}} < I_{s2}\, e^{-\frac{qV}{2kT}} = S_2\, A^* T^2 e^{-\frac{qV}{2kT}} \tag{12}$$

for the low voltages typical of the forward-biased Schottky diode ($V < \phi_{B01}$). Therefore, $I_{s1}e^{\frac{qV}{2kT}}$ can be neglected in the denominator of Equation (11), that reduces to the single SB equation

$$I_T \approx \frac{2I_{s1}I_{s2}\sin h\left(\frac{qV}{2kT}\right)}{I_{s2}e^{-\frac{qV}{2kT}}} = I_{s1}\left(e^{\frac{qV}{kT}} - 1\right) \tag{13}$$

The presence of two equally rectifying junctions is rarely found, especially in small-size devices, where there can be various effects that introduce deviation from the thermionic emission, taken into account by introducing an ideality factor n in the exponential term of Equations (3) and (4). Deviation from the ideality is caused by defects, inadvertent oxide layers, and image-force lowering that makes the SB height dependent on the applied external voltage. In such a case, the effective SBs $\phi_{B1,B2}(V)$ in Equation (5) can be written as[9,14]

$$\phi_{B1,B2}(V) = \phi_{B01,B02} \pm eV_{1,2}\left(1 - \frac{1}{n_{1,2}}\right) \tag{14}$$

where $\phi_{B01,B02}$ are the ideal SBs at zero bias, V_1 and V_2 are the voltage drops at the junctions, and $n_{1,2}$ are the ideality factors defined as $\frac{1}{n_{1,2}} = 1 \pm \frac{\partial\phi_{B1,B2}}{e\,\partial V_{1,2}}$.

Figure 2a shows I–V curve given by Equation (11) for two junctions with the same reverse saturation current and equal barrier height, at the temperature of 300 K. For both positive and negative voltages, the current saturates at the limit value set by the reverse saturation current of the reverse-biased junction. The reverse saturation current is set by the SB height as well as by junction area, as shown in Figure 2b. Indeed, imposing $S_1 = 2S_2$, two saturation currents that are one the double of the other are obtained, yielding an asymmetric I–V characteristic. Figure 2c–f shows the plots obtained substituting $\phi_{B1,B2}(V)$ from Equation (14) in Equation (11) and allowing a slight deviation from the ideal case. In these plots, we have made the simplifying assumption that $V_1 = V_2 = \frac{V}{2}$

Figure 2c, in particular, shows that despite the reverse-bias of one of the two junctions, the current does not saturate at positive or negative bias due to the dependence of the barrier on the applied voltage. Such behavior is much more similar to what is usually observed in practical devices. Furthermore, if we consider also different junction areas, the current can increase with different trends, as shown in Figure 2d. In particular, the current is more limited by the junction with the narrower area. Figure 2e,f shows the I–V curves from Equation (11) with different SB heights and ideality factors. We note that in Figure 2e the current is lower at positive voltage because the

© 2020 Wiley-VCH GmbH

2199160x, 2021, 2, Downloaded from https://onlinelibrary.wiley.com/doi/10.1002/aelm.202000979 by Universita Di Salerno, Wiley Online Library on [20/01/2025]. See the Terms and Conditions (https://onlinelibrary.wiley.com/terms-and-conditions) on Wiley Online Library for rules of use; OA articles are governed by the applicable Creative Commons License

2199160x, 2021, 2, Downloaded from https://onlinelibrary.wiley.com/doi/10.1002/aelm.202000979 by Universita Di Salerno, Wiley Online Library on [20/01/2025]. See the Terms and Conditions (https://onlinelibrary.wiley.com/terms-and-conditions) on Wiley Online Library for rules of use; OA articles are governed by the applicable Creative Commons License

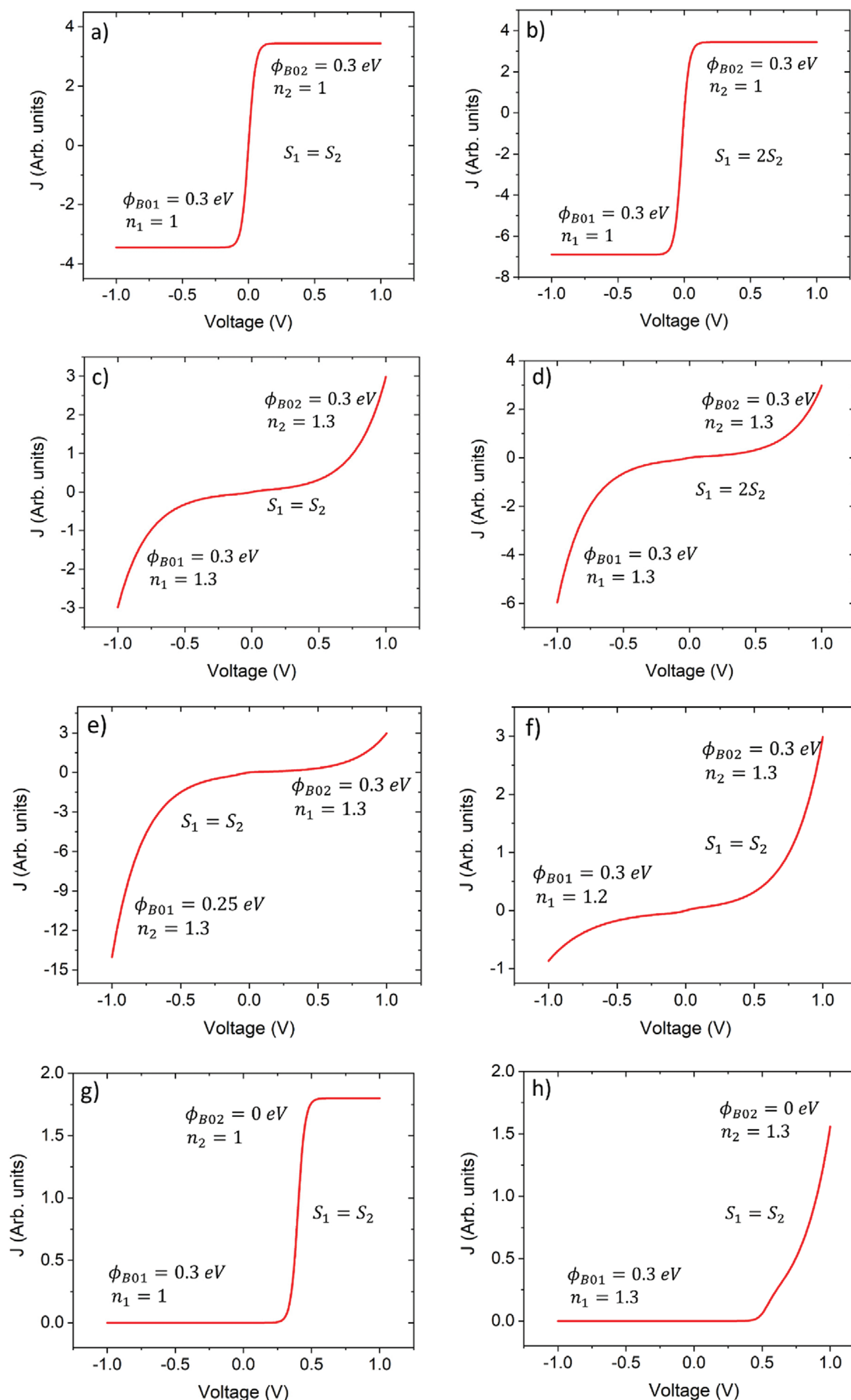

Figure 2. a–h) Simulation of Equation (11) describing the current in two back-to-back Schottky junctions. a) *I–V* characteristic for contacts with the same barrier height, $\phi_{B01} = \phi_{B02} = 0.3$ eV, the same junction area $S_1 = S_2$, and perfect ideality ($n = 1$). The current saturates to the reverse saturation current of the reverse-biased diode. b) *I–V* characteristic for $\phi_{B01} = \phi_{B02} = 0.3$ eV, perfect ideality ($n = 1$), and $S_1 = 2S_2$; the saturated currents are $I_{S2} = 2I_{S1}$. c) *I–V* characteristic for $\phi_{B01} = \phi_{B02} = 0.3$ eV, areas $S_1 = S_2$, and ideality factors $n_1 = n_2 = 1.3$. The ideality factor is due to the image force barrier lowering. The current does not saturate because the reverse biased diode is affected by image force barrier lowering. d) *I–V* characteristic for $\phi_{B01} = \phi_{B02} = 0.3$ eV, areas $S_1 = 2S_2$, and ideality factors $n_1 = n_2 = 1.3$. We observe that the current is lower when limited by the narrower junction. e) *I–V* characteristic for $\phi_{B01} = 0.25$ eV, $\phi_{B02} = 0.3$ eV, areas $S_1 = S_2$, and ideality factors $n_1 = n_2 = 1.3$. The current results more limited at positive voltage because it is strongly

 © 2020 Wiley-VCH GmbH

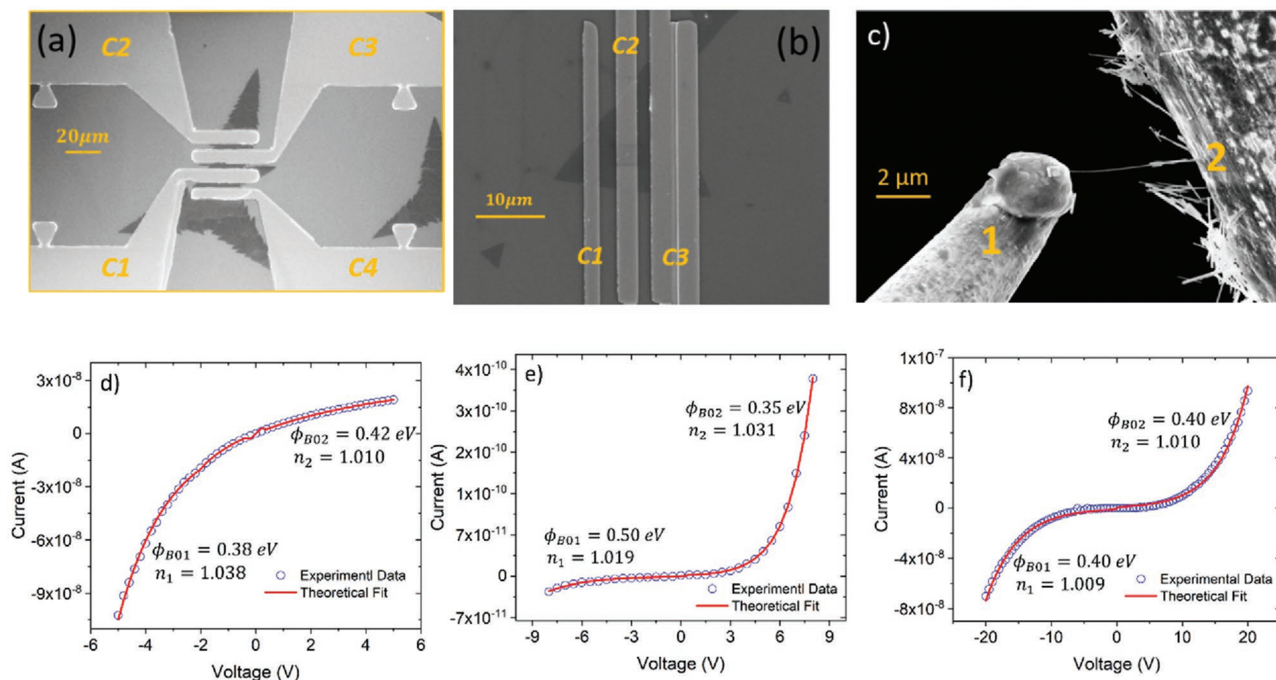

Figure 3. a) SEM image of a MoS_2 flake contacted with four Ti/Au leads. b) SEM image of a WSe_2 flake covered with Ni/Au contacts. c) SEM image showing a single WS_2 nanotube contacted by two tungsten tips, marked as 1 and 2, respectively. d–f) *I–V* characteristic of the MoS_2, WSe_2, and WS_2 devices. The blue circles represent the experimental data, while the red lines are the fitting curves from Equation (11), with the SB height and the ideality factor as fitting parameters.

current is limited by the higher ϕ_{B02} barrier (in contrast, at negative voltage the current is limited by the lower ϕ_{B01} barrier). Figure 2f shows the current behavior in a device where the two Schottky junctions have the same barrier heights but different ideality factors. In this case, the current is lower when is limited by the junction with the lower ideality factor, i.e., by the barrier closer to the ideal SB.

Figure 2g,h shows *I–V* curves given by Equation (11) setting $\phi_{B01} \neq \phi_{B02} = 0$. The classic current behavior for a single SB is obtained for both ideal and image-force lowered barriers.

3. Results and Discussion

In recent years, nanostructured materials have attracted significant attention owing to their unique electrical, optical, and mechanical properties.[15–19] 1D and 2D nanomaterials present atomic dimensions that enable aggressive length scaling in the future generation of electronic devices like field effect transistors[20–23] and memory devices.[24–27] Despite the huge progresses, the realization of reliable contacts with nanostructured materials poses substantial issues[28–30] that hamper the understanding of the intrinsic electric transport properties and the exploitation of the nanomaterials in electronic and optoelectronic applications. Contacts are the communication links between the nanomaterials and the outer world, and the fabrication of Ohmic contacts with linear current–voltage characteristics and low-resistance is still an open challenge.[30–32] One of the main problems is the lack of reproducibility as contacts realized under the same conditions and using the same metals can have different electrical characteristics ranging from Schottky to Ohmic behavior.[33] Moreover, the contacts can influence the conduction mechanism inside a device contributing to the change from the typical thermally activated band conduction to variable range hopping or space charge limited current.[34–36]

Figure 3a–c shows the scanning electron microscope (SEM) images of three nanodevices: the first is a MoS_2 flake contacted with four Ti/Au leads,[37] the second is a WSe_2 flake covered with Ni/Au contacts,[23] and the third is a single WS_2 nanotube stuck to two tungsten tips due to van der Waals interaction.[38] MoS_2 and WSe_2 flakes lay on an electrically grounded SiO_2/p-Si substrate, while WS_2 nanotube is suspended between the two tungsten tips. The details of the fabrication, characterization, and electrical measurements can be found elsewhere.[23,37,38]

Figure 3d shows the *I–V* characteristic of the MoS_2 nanosheet with strongly asymmetric behavior. This result confirms that contacts made simultaneously and under the same

limited by the higher ϕ_{B02} barrier. f) *I–V* characteristic for $\phi_{B01} = \phi_{B02} = 0.3$ eV, areas $S_1 = S_2$, and ideality factor $n_1 = 1.2$ and $n_2 = 1.3$. The current is limited at negative voltage because of the higher blocking effect of ϕ_{B01}, that is closer to an ideal barrier. g) *I–V* characteristic for $\phi_{B01} \neq \phi_{B02} = 0$ eV, areas $S_1 = S_2$, and perfect ideality ($n_1 = n_2 = 1$). The current of a single ideal SB is obtained at low forward bias ($V < \phi_{B01}$). h) *I–V* characteristic for $\phi_{B01} \neq \phi_{B02} = 0$ eV, areas $S_1 = S_2$, and $n_1 = n_2 = 1.3$. The negative current is still very low, but the slope of the *I–V* curve is voltage dependent.

© 2020 Wiley-VCH GmbH

2199160x, 2021, 2, Downloaded from https://onlinelibrary.wiley.com/doi/10.1002/aelm.202000979 by Universita Di Salerno, Wiley Online Library on [20/01/2025]. See the Terms and Conditions (https://onlinelibrary.wiley.com/terms-and-conditions) on Wiley Online Library for rules of use; OA articles are governed by the applicable Creative Commons License

conditions can have different barrier height (the contact area is about the same). Figure 3d also shows the curve obtained from Equation (11), superposed to the experimental data, demonstrating the excellent fitting. The results of the fit confirm the presence of two different barriers at the contacts that occur to be $\phi_{B01} = 0.38$ eV and $\phi_{B02} = 0.42$ eV with ideality factor $n_1 = 1.038$ and $n_2 = 1.010$, respectively. From the literature, the MoS_2 electron affinity ranges from 3.74 to 4.45 eV,[39–41] while Ti work function is 4.33 eV. According to Equation (1), the SB height should range from –0.12 to 0.59 eV where the negative values can be considered as the Ohmic contacts. We highlight how Equation (1), also known as the Schottky–Mott rule, does not yield an accurate estimate of the barrier, especially for 2D materials. Indeed, the Schottky–Mott model does not take into account the pinning of the Fermi level which may occur at both interfaces, even in an asymmetrical way. For this reason, it can only be used as a qualitative method to obtain the rough estimation of the SB. Moreover, our results are comparable with the SB height ranging from 0.31 to 0.51 eV experimentally determined in previous works.[6]

Figure 3e shows the I–V characteristic of the WSe_2 flake that presents a strong asymmetric behavior. As expected, the fit yields two different values for the SB heights, namely, $\phi_{B01} = 0.50$ eV and $\phi_{B02} = 0.35$ eV with ideality factor $n_1 = 1.019$ and $n_2 = 1.031$, respectively. In this case, considering that the Ni work function is about 5.0 eV while the WSe_2 electron affinity is about 3.7 eV,[42] the results from the fit of Equation (11) is not consistent with of Equation (1), that would give the unrealistic high barrier of 1.3 eV.

Figure 3f shows the I–V characteristic of the nanowire of Figure 3c. The I–V curve is symmetric pointing to the presence of two equal barriers. The fit of Equation (11) perfectly reproduces the experimental data and allows the estimation of the SB height as $\phi_{B01} = \phi_{B02} = 0.40$ eV with the ideality factor $n_1 = 1.009$ and $n_2 = 1.010$, respectively. In this case, considering χ_s (WS_2) = 4.5 eV[43] and ϕ_M (W) = 4.32 − 5.22 eV, the estimated barrier is within the range predicted by Equation (1), that is –0.18 to 0.72 eV.

4. Conclusion

In conclusion, we have proposed a simple model to describe the I–V characteristics of a generic semiconductor device with two Schottky junctions at the contacts. The model includes non-idealities that make the barrier height dependent on the applied voltage. We have shown that the model can account for several experimental observation and fully reproduce both symmetric and asymmetric characteristics. Finally, we have tested the model by fitting the I–V characteristics of devices with MoS_2 and WSe_2 nanosheets and WS_2 nanotubes. The model not only perfectly reproduces the experimental data but also allows to simultaneously extract the two contact barriers and their respective ideality factors.

Conflict of Interest

The authors declare no conflict of interest.

Keywords

current–voltage characteristic, diodes, Schottky barriers, transition metal dichalcogenides

Received: October 8, 2020
Revised: November 18, 2020
Published online: December 28, 2020

[1] W. G. Oldham, A. G. Milnes, *Solid-State Electron.* **1964**, *7*, 153.
[2] F. Hernández-Ramírez, A. Tarancón, O. Casals, J. Rodríguez, A. Romano-Rodríguez, J. R. Morante, S. Barth, S. Mathur, T. Y. Choi, D. Poulikakos, V. Callegari, P. M. Nellen, *Nanotechnology* **2006**, *17*, 5577.
[3] T. Nagano, M. Tsutsui, R. Nouchi, N. Kawasaki, Y. Ohta, Y. Kubozono, N. Takahashi, A. Fujiwara, *J. Phys. Chem. C* **2007**, *111*, 7211.
[4] R. Nouchi, *J. Appl. Phys.* **2014**, *116*, 184505.
[5] A. J. Chiquito, C. A. Amorim, O. M. Berengue, L. S. Araujo, E. P. Bernardo, E. R. Leite, *J. Phys.: Condens. Matter* **2012**, *24*, 225303.
[6] A. Di Bartolomeo, A. Grillo, F. Urban, L. Iemmo, F. Giubileo, G. Luongo, G. Amato, L. Croin, L. Sun, S.-J. Liang, L. K. Ang, *Adv. Funct. Mater.* **2018**, *28*, 1800657.
[7] A. Di Bartolomeo, F. Urban, M. Passacantando, N. McEvoy, L. Peters, L. Iemmo, G. Luongo, F. Romeo, F. Giubileo, *Nanoscale* **2019**, *11*, 1538.
[8] A. Di Bartolomeo, F. Giubileo, A. Grillo, G. Luongo, L. Iemmo, F. Urban, L. Lozzi, D. Capista, M. Nardone, M. Passacantando, *Nanomaterials* **2019**, *9*, 1598.
[9] S. M. Sze, K. K. Ng, *Physics of Semiconductor Devices*, Wiley-Interscience, Hoboken, NJ **2007**.
[10] F. Urban, F. Giubileo, A. Grillo, L. Iemmo, G. Luongo, M. Passacantando, T. Foller, L. Madauß, E. Pollmann, M. P. Geller, D. Oing, M. Schleberger, A. Di Bartolomeo, *2D Mater.* **2019**, *6*, 045049.
[11] A. Grillo, F. Giubileo, L. Iemmo, G. Luongo, F. Urban, M. Passacantando, A. Di Bartolomeo, *Mater. Today: Proc.* **2020**, *20*, 64.
[12] A. Di Bartolomeo, A. Pelella, F. Urban, A. Grillo, L. Iemmo, M. Passacantando, X. Liu, F. Giubileo, *Adv. Electron. Mater.* **2020**, *6*, 2000094.
[13] K. Sotthewes, R. van Bremen, E. Dollekamp, T. Boulogne, K. Nowakowski, D. Kas, H. J. W. Zandvliet, P. Bampoulis, *J. Phys. Chem. C* **2019**, *123*, 5411.
[14] A. Di Bartolomeo, F. Giubileo, G. Luongo, L. Iemmo, N. Martucciello, G. Niu, M. Fraschke, O. Skibitzki, T. Schroeder, G. Lupina, *2D Mater.* **2016**, *4*, 015024.
[15] B. K. Teo, X. H. Sun, *Chem. Rev.* **2007**, *107*, 1454.
[16] T. Jin, Q. Han, Y. Wang, L. Jiao, *Small* **2018**, *14*, 1703086.
[17] Z. Zhou, Y. Cui, P.-H. Tan, X. Liu, Z. Wei, *J. Semicond.* **2019**, *40*, 061001.
[18] A. Di Bartolomeo, *Nanomaterials* **2020**, *10*, 579.
[19] K. Khan, A. K. Tareen, M. Aslam, R. Wang, Y. Zhang, A. Mahmood, Z. Ouyang, H. Zhang, Z. Guo, *J. Mater. Chem. C* **2020**, *8*, 387.
[20] A. D. Bartolomeo, M. Rinzan, A. K. Boyd, Y. Yang, L. Guadagno, F. Giubileo, P. Barbara, *Nanotechnology* **2010**, *21*, 115204.
[21] D. Tran, T. Pham, B. Wolfrum, A. Offenhäusser, B. Thierry, *Materials* **2018**, *11*, 785.
[22] T. Roy, M. Tosun, J. S. Kang, A. B. Sachid, S. B. Desai, M. Hettick, C. C. Hu, A. Javey, *ACS Nano* **2014**, *8*, 6259.
[23] A. Di Bartolomeo, F. Urban, M. Passacantando, N. McEvoy, L. Peters, L. Iemmo, G. Luongo, F. Romeo, F. Giubileo, *Nanoscale* **2019**, *11*, 1538.

 © 2020 Wiley-VCH GmbH

2199160x, 2021, 2, Downloaded from https://onlinelibrary.wiley.com/doi/10.1002/aelm.202000979 by Universita Di Salerno, Wiley Online Library on [20/01/2025]. See the Terms and Conditions (https://onlinelibrary.wiley.com/terms-and-conditions) on Wiley Online Library for rules of use; OA articles are governed by the applicable Creative Commons License

[24] S. Bertolazzi, P. Bondavalli, S. Roche, T. San, S.-Y. Choi, L. Colombo, F. Bonaccorso, P. Samorì, *Adv. Mater.* **2019**, *31*, 1806663.
[25] A. Di Bartolomeo, Y. Yang, M. B. M. Rinzan, A. K. Boyd, P. Barbara, *Nanoscale Res. Lett.* **2010**, *5*, 1852.
[26] T. Qu, Y. Sun, M. Chen, Z. Liu, Q. Zhu, B. Wang, T. Zhao, C. Liu, J. Tan, S. Qiu, Q. Li, Z. Han, W. Wang, H. Cheng, D. Sun, *Adv. Mater.* **2020**, *32*, 1907288.
[27] A. Di Bartolomeo, H. Rücker, P. Schley, A. Fox, S. Lischke, K.-Y. Na, *Solid-State Electron.* **2009**, *53*, 644.
[28] F. Giubileo, A. Di Bartolomeo, *Prog. Surf. Sci.* **2017**, *92*, 143.
[29] A. Di Bartolomeo, *Phys. Rep.* **2016**, *606*, 1.
[30] F. Léonard, A. A. Talin, *Nat. Nanotechnol.* **2011**, *6*, 773.
[31] F. Urban, G. Lupina, A. Grillo, N. Martucciello, A. Di Bartolomeo, *Nano Express* **2020**, *1*, 010001.
[32] D. S. Schulman, A. J. Arnold, S. Das, *Chem. Soc. Rev.* **2018**, *47*, 3037.
[33] H. S. Yoon, H.-E. Joe, S. Jun Kim, H. S. Lee, S. Im, B.-K. Min, S. C. Jun, *Sci. Rep.* **2015**, *5*, 10440.
[34] A. Grillo, F. Giubileo, L. Iemmo, G. Luongo, F. Urban, A. Di Bartolomeo, *J. Phys.: Conf. Ser.* **2019**, *1226*, 012013.
[35] A. J. Chiquito, A. J. C. Lanfredi, R. F. M. de Oliveira, L. P. Pozzi, E. R. Leite, *Nano Lett.* **2007**, *7*, 1439.
[36] A. Grillo, A. Di Bartolomeo, F. Urban, M. Passacantando, J. M. Caridad, J. Sun, L. Camilli, *ACS Appl. Mater. Interfaces* **2020**, *12*, 12998.
[37] A. Pelella, O. Kharsah, A. Grillo, F. Urban, M. Passacantando, F. Giubileo, L. Iemmo, S. Sleziona, E. Pollmann, L. Madauß, M. Schleberger, A. Di Bartolomeo, *ACS Appl. Mater. Interfaces* **2020**, *12*, 40532.
[38] A. Grillo, M. Passacantando, A. Zak, A. Pelella, A. Di Bartolomeo, *Small* **2020**, *16*, 2002880.
[39] M. Sup Choi, G.-H. Lee, Y.-J. Yu, D.-Y. Lee, S. Hwan Lee, P. Kim, J. Hone, W. Jong Yoo, *Nat. Commun.* **2013**, *4*, 1624.
[40] S. Das, H.-Y. Chen, A. V. Penumatcha, J. Appenzeller, *Nano Lett.* **2013**, *13*, 100.
[41] S. McDonnell, R. Addou, C. Buie, R. M. Wallace, C. L. Hinkle, *ACS Nano* **2014**, *8*, 2880.
[42] Y. Liang, S. Huang, R. Soklaski, L. Yang, *Appl. Phys. Lett.* **2013**, *103*, 042106.
[43] A. Kuc, N. Zibouche, T. Heine, *Phys. Rev. B* **2011**, *83*, 245213.

© 2020 Wiley-VCH GmbH

2199160x, 2021, 2, Downloaded from https://onlinelibrary.wiley.com/doi/10.1002/aelm.202000979 by Universita Di Salerno, Wiley Online Library on [20/01/2025]. See the Terms and Conditions (https://onlinelibrary.wiley.com/terms-and-conditions) on Wiley Online Library for rules of use; OA articles are governed by the applicable Creative Commons License